Modeling the Effect of Shear Stress on Deposition from "Waxy" Mixtures under Laminar Flow with Heat Transfer †

ARTICLE *in* ENERGY & FUELS · MAY 2007

Impact Factor: 2.79 · DOI: 10.1021/ef060445u

2 AUTHORS, INCLUDING:

Anil K Mehrotra
The University of Calgary
160 PUBLICATIONS **2,348** CITATIONS

Modeling the Effect of Shear Stress on Deposition from "Waxy" Mixtures under Laminar Flow with Heat Transfer†

Anil K. Mehrotra* and Nitin V. Bhat

Department of Chemical and Petroleum Engineering, University of Calgary, Calgary, Alberta, Canada T2N 1N4

Received September 1, 2006. Revised Manuscript Received October 26, 2006

A mathematical model is presented for solids deposition from multicomponent "waxy" mixtures under laminar flow in a small double-pipe heat exchanger. The model is based primarily on the moving boundary problem approach involving heat transfer with a phase change. A novel formulation based on the one-dimensional deformation of a cubical cage is proposed for incorporating the effect of shear stress on the deposition process. It is postulated that the application of shear stress causes tilting of the cubical cage, which leads to the release of a portion of the liquid phase. The tilted-cage deformation angle is estimated by matching the deposit-layer composition data from two recent experimental studies. A change in the deformation angle is predicted to result in a shift in the carbon-number distribution of the deposit. The shear stress is predicted to cause a wax enrichment of the deposit layer without affecting the deposit-layer thickness, which is governed mainly by heat-transfer and phase equilibrium considerations. The estimated deformation angle is shown to depend upon the fractional deposit thermal resistance (or the fractional temperature drop), deposit mass, and Reynolds number. The results of this study confirm that the deposition process is primarily thermally driven, while the deposit composition is influenced by shear stress and thermodynamic considerations.

Introduction

The adverse effects of wax deposition are encountered in all sectors of the petroleum industry, ranging from the damage to oil reservoir formations to the blockage of pipelines and process equipment. The presence of deposited solids causes an increased pressure drop and/or a decreased flow rate.

When paraffinic mixtures, such as "waxy" crude oils, flowing through a pipeline are exposed to temperatures below their wax appearance temperature (WAT), solids deposition on the pipe wall is known to occur. This is because heavier paraffins (or waxes) have a reduced solubility in the liquid phase at lower temperatures, causing their crystallization and deposition on the cooler pipe wall. The deposit layer is comprised of liquid and solid phases in a gel-like structure, whose composition and relative proportions vary across the deposit thickness because of the variations in temperature, concentration, and shear stress.

Paraffinic mixtures display complex rheological behavior, which changes considerably upon cooling from essentially Newtonian behavior at temperatures above their WAT to the time-dependent, non-Newtonian characteristics, with orders-of-magnitude increases in the apparent viscosity, between the WAT and the pour point temperature (PPT).[1−3] It has been shown that the rheological behavior of prepared waxy mixtures changes with temperature, i.e., from Newtonian to shear thinning to apparently plastic at lower temperatures.[4] At temperatures below the PPT, waxy mixtures have been noted to behave as weakly attractive colloidal gels; the structural build-up resulting from the crystal formation and aggregation was favored by lower temperatures and longer times.[4,5] Furthermore, the mechanical history has been reported to exert significant effects on the structural conditions and the rheological properties during the gel-formation process and in its final state. Even small deformations and stresses can affect the aggregation of paraffin crystals during gel formation.[4]

The deposition of solids from "waxy" mixtures is a complex phenomenon, for which several different models or approaches have been proposed.[6] Among these, the molecular diffusion approach has been used in several studies on solids deposition from "waxy" mixtures and crude oils.[7−13] The molecular diffusion approach is based on the premise that the crude oil

† Presented at the 7th International Conference on Petroleum Phase Behavior and Fouling.

* To whom correspondence should be addressed. Telephone: (403) 220-7406. Fax: (403) 284-4852. E-mail: mehrotra@ucalgary.ca.

(1) Wardhaugh, L. T.; Boger, D. V. Measurement of the Unique Flow Properties of Waxy Crude Oils. *Chem. Eng. Res. Des.* **1987**, *65*, 74.

(2) Pederson, K. S.; Ronningsen, H. P. Effect of Precipitated Wax on Viscosity. A Model for Predicting Non-Newtonian Viscosity of Crude Oils. *Energy Fuels* **2000**, *14*, 43.

(3) Tiwary, D.; Mehrotra, A. K. Phase Transformation and Rheological Behaviour of Highly Paraffinic "Waxy" Mixtures. *Can. J. Chem. Eng.* **2004**, *82*, 162.

(4) Visintin, R. F. G.; Lapasin, R.; Vignati, E.; D'Antona, P.; Lockhart, T. P. Rheological Behavior and Structural Interpretation of Waxy Crude Oil Gels. *Langmuir* **2005**, *21*, 6240.

(5) Vignati, E.; Piazza, R.; Visintin, R. F. G.; Lapasin, R.; D'Antona, P.; Lockhart, T. P. Wax Crystallization and Aggregation in a Model Crude Oil. *J. Phys.: Condens. Matter* **2005**, *17*, S3651.

(6) Azevedo, L. F. A.; Teixeira, A. M. A Critical Review of the Modeling of Wax Deposition Mechanisms. *Pet. Sci. Technol.* **2003**, *21*, 393.

(7) Burger, E. D.; Perkins, T. K.; Striegler, J. H. Studies of Wax Deposition in the Trans Alaska Pipeline. *J. Pet. Technol.* **1981**, *33*, 1075.

(8) Svendsen, J. A. Mathematical Modeling of Wax Deposition in Oil Pipeline Systems. *AIChE J.* **1993**, *39*, 1377.

(9) Creek, J. L.; Lund, H. J.; Brill, J. P.; Volk, M. Wax Deposition in Single Phase Flow. *Fluid Phase Equilib.* **1999**, *801*, 158−160.

(10) Kok, M. V.; Saracoglu, R. O. Mathematical Modeling of Wax Deposition in Crude Oil Pipelines (Comparative Study). *Pet. Sci. Technol.* **2000**, *18*, 1121.

(11) Singh, P.; Venkatesan, R.; Fogler, H. S.; Nagarajan, N. Formation and Aging of Incipient Thin Film Wax−Oil Gels. *AIChE J.* **2000**, *46*, 1059.

(12) Singh, P.; Venkatesan, R.; Fogler, H. S.; Nagarajan, N. Morphological Evolution of Thick Wax Deposits during Aging. *AIChE J.* **2001**, *47*, 6.

10.1021/ef060445u CCC: $37.00
Published on Web 12/13/2006

flow in a pipe with the wall temperature below the WAT provides a radial temperature gradient, which creates a radial concentration gradient. The deposit layer is assumed to be formed on the cooler surface because of the reduced solubility of paraffins at lower temperatures. The mass of deposited wax has been reported to decrease with an increasing flow rate under both laminar and turbulent flows.[12,14−17] Other studies have addressed related topics such as the deposit removal by shear, the deposit aging, and the effect of the flow or shear rate.[9,11,18,19] Also, the deposit composition and "hardness" have been observed to vary with time through a process referred to as "deposit aging".[9,11,15,16,18,20,21]

In addition to the role of molecular diffusion, the importance of heat transfer in the deposition process has also been identified in several studies.[9,14−16,19,22,23] Recent laboratory investigations with prepared paraffinic mixtures have reported the deposition process to be a relatively fast process, with the thermal steady state accomplished within 30 min.[15−17] Beyond this time, the concentration of heavier paraffins in the deposit layer was observed to increase slightly. Although the overall temperature difference between the paraffinic mixture and the surroundings is generally accepted to provide the driving force for solids deposition, it was shown that the temperature difference across the deposit layer is a controlling parameter.[15−17]

The hardening and compositional changes that occur within the deposit layer with time lead to its aging, which has been interpreted in terms of the paraffin molecules below the critical carbon number diffusing out of the deposit, while those above it diffusing into the deposit through a counter-diffusion process.[20] It was pointed out that this aging process depended upon the operating conditions such that it was a stronger function of the temperature difference across the deposit than the compressive force as a result of flow. The deposit aging process has also been interpreted through Ostwald ripening, which relates to a self-organization of wax molecules based on their area/size ratio.[21]

Of particular relevance to this study are two recent experimental studies on the deposition of solids from wax−solvent mixtures under laminar flow in small counter-current heat exchangers.[15,16,24,25] These laboratory studies were carried out with prepared mixtures of a multicomponent wax dissolved in *n*-dodecane ($C_{12}H_{26}$)[15,24] and Norpar13 (a mixed paraffinic solvent).[16,25] The variables in these two studies were the wax concentration, the inlet hot and cold stream temperatures, the "hot" stream flow rate (or Reynolds number), and the deposition time. The transfer of thermal energy from the "hot" wax−solvent mixture to the "cold" coolant (water) was shown to involve four thermal resistances in series. These were the convective resistance of the "hot" stream, R_h; the conductive resistance of the deposit layer, R_d; the conductive resistance of the metal tube wall, R_m; and the convective resistance of the "cold" stream, R_c.[15,16] A dimensionless parameter, θ_d, was defined as the ratio of the thermal resistance of the deposit layer to the combined thermal resistances at the steady state, i.e., $\theta_d = (R_d)/(R_h + R_d + R_m + R_c)$.[15] It was shown that θ_d is also equal to the fractional temperature drop across the deposit layer. The mass of deposited solids was related to θ_d for all solvent−wax mixtures in each case.[15,16] Predictions from the steady-state heat-transfer model were shown to be in good agreement with the data, which indicated the deposition process to be controlled primarily by heat transfer. Also reported were the gas chromatography (GC) analyses for selected deposit samples.

Very briefly, the first experimental study[15,24] was carried out in a batch apparatus, in which the flow of the "hot" wax−C_{12} mixture was accomplished with an axial-flow propeller, while the deposition took place on the inner "cold" surface of a 4.8 cm long copper tube with a 2.64 cm inside diameter. Table 1 summarizes the experimental conditions and results for the 2 h experiments for which the deposit sample analyses were available.[24] The second experimental study[16,25] was performed in a bench-scale flow-loop apparatus, consisting of a counter-current double-pipe heat exchanger. The deposition took place on the inner surface of a 10.8 cm long aluminum tube with a 2.54 cm inside diameter, while the coolant flowed through the annular region. The GC analyses of the deposit layer showed a significant shift in the carbon-number distribution. The C_{20}^+ content of the deposit layer was higher, by 70−200%, than that of the corresponding wax−solvent mixture. Table 2 summarizes the experimental conditions and results for the 4 h experiments for which the deposit sample analyses were available.[25] The results of these two studies[15,16,24,25] are used for validating a model developed to account for the effect of shear stress on deposit formation and growth and for predicting the deposit-layer composition.

The mathematical framework for the sheared-deposition model presented in this study extends a recently proposed model based on the moving boundary problem approach for deposition in radial and axial directions of a pipe under static and laminar flow conditions.[22,23] It was shown that the phase transformation at the liquid−deposit interface and heat transfer in the liquid and deposit regions primarily control the deposit-layer growth until reaching the steady state.

A cubical-cage representation is developed for the relative amounts of liquid and solid phases in the deposit. It is postulated that the shear stress causes a certain extent of plastic deformation of the cubical cage, which releases a portion of the trapped liquid as the deposit layer is formed. The fraction of the liquid released from the cubical cage during its formation at the liquid−deposit interface was estimated by matching the experimental deposit

(13) Ramirez-Jaramillo, E.; Lira-Galeana, C.; Manero, O. Modeling Wax Deposition in Pipelines. *Pet. Sci. Technol.* **2004**, *22*, 821.
(14) Wu, C.; Wang, K. S.; Shuler, P. J.; Tand, Y.; Creek, J. L.; Carlson, R. M.; Cheung, S. Measurement of Wax Deposition in Paraffin Solutions. *AIChE J.* **2002**, *48*, 2107.
(15) Bidmus, H. O.; Mehrotra, A. K. Heat-Transfer Analogy for Wax Deposition from Paraffinic Mixtures. *Ind. Eng. Chem. Res.* **2004**, *43*, 791.
(16) Parthasarathi, P.; Mehrotra, A. K. Solids Deposition from Multicomponent Wax−Solvent Mixtures in a Benchscale Flow-Loop Apparatus with Heat Transfer. *Energy Fuels* **2005**, *19*, 1387.
(17) Fong, N. F.; Mehrotra, A. K. Deposition from Wax−Solvent Mixtures in a Flow-Loop Apparatus: Extension of Heat-Transfer Analogy to Turbulent Flow. *Energy Fuels* **2007**, in press.
(18) Singh, P.; Venkatesan, R.; Fogler, H. S.; Nagarajan, N. Prediction of the Wax Content of the Incipient Wax−Oil Gel in a Pipeline: An Application of the Controlled Stress Rheometer. *J. Rheol.* **1999**, *43*, 1437.
(19) Bott, T. R.; Gudmunsson, J. S. Deposition of Paraffin Wax from Kerosene in Cooled Heat Exchanger Tubes. *Can. J. Chem. Eng.* **1977**, *55*, 381.
(20) Singh., P.; Youyen, A; Fogler, H. S. Existence of a Critical Carbon Number in the Aging of a Wax−Oil Gel. *AIChE J.* **2001**, *47*, 2111.
(21) Coutinho, J. A. P.; Lopes da Silva, J. A.; Ferreira, A.; Soares, M. R.; Daridon, J. L. Evidence for the Aging of Wax Deposits in Crude Oils by Ostwald Ripening. *Pet. Sci. Technol.* **2003**, *21*, 381.
(22) Bhat, N. V.; Mehrotra, A. K. Modeling of Deposit Formation from "Waxy" Mixtures via Moving Boundary Formulation: Radial Heat Transfer under Static and Laminar Flow Conditions. *Ind. Eng. Chem. Res.* **2005**, *44*, 6948.
(23) Bhat, N. V.; Mehrotra, A. K. Modeling of Deposition from "Waxy" Mixtures in a Pipeline under Laminar Flow Conditions via Moving Boundary Formulation. *Ind. Eng. Chem. Res.* **2006**, *45*, 8728.
(24) Bidmus, H. O. A Thermal Study of Wax Deposition from Paraffinic Mixtures. M.Sc. Thesis, University of Calgary, Calgary, Canada, 2003.
(25) Parthasarathi, P. Deposition and Aging of Waxy Solids from Paraffinic Mixtures. M.Sc. Thesis, University of Calgary, Calgary, Canada, 2004.

Table 1. Summary of the Experimental Data[15,24] and Estimated Deformation Angle, β, for Deposition from Wax−$C_{12}H_{26}$ Mixtures under Laminar Flow

wax concentration in wax−$C_{12}H_{26}$ mixtures (mass %)	average Re	T_{hi} (°C)	T_{ci} (°C)	θ_d	Ω (kg m^{-2})	k_d (W m^{-1} K^{-1})	Φ	estimated β
10 mass %	500	WAT + 3	WAT − 17	0.85	2.00	0.24	1.62	79.4
(WAT = 27.0 °C)		WAT + 3	WAT − 12	0.80	1.54	0.23	1.58	77.6
		WAT + 8	WAT − 17	0.68	1.08	0.26	2.27	83.0
		WAT + 8	WAT − 12	0.60	0.76	0.27	2.92	85.6
	150	WAT + 3	WAT − 17	0.85	3.24	0.19	1.25	65.0
		WAT + 3	WAT − 12	0.80	0.41	0.20	1.19	62.4
		WAT + 8	WAT − 17	0.68	1.18	0.24	1.30	65.4
		WAT + 8	WAT − 12	0.60	0.77	0.24	1.27	65.2
15 mass %	500	WAT + 9	WAT − 16	0.64	0.77	0.25	1.05	36.6
(WAT = 31.0 °C)		WAT + 9	WAT − 11	0.55	0.46	0.29	1.05	39.0
	150	WAT + 4	WAT − 11	0.73	1.37	0.17	1.07	44.6
20 mass %	500	WAT + 9	WAT − 15	0.63	0.76	0.30	1.01	16.0
(WAT = 34.0 °C)		WAT + 4	WAT − 8	0.67	1.35	0.29	1.04	38.7
	150	WAT + 4	WAT − 15	0.79	1.76	0.21	1.14	46.6

Table 2. Summary of the Experimental Data[16,25] and Estimated Deformation Angle, β, for Deposition from Wax−Norpar13 Mixtures under Laminar Flow

wax concentration in wax−Norpar13 mixtures (mass %)	average Re	T_{hi} (°C)	T_{ci} (°C)	θ_d	Ω (kg m^{-2})	k_d (W m^{-1} K^{-1})	Φ	estimated β
7 mass %	1000	WAT + 5	WAT − 10	0.70	1.70	0.25	1.72	80.0
(WAT = 24.5 °C)		WAT + 10	WAT − 10	0.47	0.90	0.33	2.18	82.2
		WAT + 5	WAT − 5	0.51	0.99	0.32	1.96	82.2
	600	WAT + 5	WAT − 10	0.67	1.67	0.26	1.69	79.0
10 mass %	1000	WAT + 5	WAT − 10	0.62	1.20	0.22	1.81	80.0
(WAT = 28.0 °C)		WAT + 10	WAT − 10	0.45	0.70	0.25	2.71	84.5
		WAT + 5	WAT − 5	0.47	0.75	0.25	2.23	83.4
	600	WAT + 5	WAT − 10	0.63	1.37	0.23	1.62	77.8
12.5 mass %	1000	WAT + 5	WAT − 10	0.59	1.03	0.19	2.30	83.9
(WAT = 30.5 °C)		WAT + 10	WAT − 10	0.40	0.65	0.26	2.47	84.1
	600	WAT + 5	WAT − 10	0.57	1.14	0.23	1.86	82.8
15 mass %	1000	WAT + 5	WAT − 10	0.62	1.15	0.23	1.71	79.5
(WAT = 32.0 °C)		WAT + 10	WAT − 10	0.42	0.68	0.30	2.94	85.4
		WAT + 5	WAT − 5	0.38	0.60	0.30	1.87	81.4
	600	WAT + 5	WAT − 10	0.62	1.30	0.24	1.70	78.9

composition. Thus, the proposed sheared-deposition model incorporates the effect of shear stress as a result of the flowing liquid on the deposition process and deposit characteristics. The predictions for the carbon-number distribution in the deposit layer are shown to compare well with the experimental data.[15,16,24,25] The predictions are used to identify relationships between the deformation angle and the deposition and flow characteristics.

Model Development

In this section, a mathematical framework is presented for the formation and growth of the deposit layer from the cooling of a wax−solvent mixture, flowing through a tube under laminar flow, in terms of the moving boundary problem formulation. The solid−liquid-phase equilibrium considerations are incorporated using the thermodynamic model of Coutinho.[26]

Deposition in a Short Tube with Heat Transfer. A mathematical model for the deposition from a waxy mixture in radial and axial directions of a pipe has been described previously.[22,23] The same approach is adapted to the geometrical arrangement described below, which is similar to that used in the two laboratory studies.[15,16]

Consider the laminar flow of a "hot" wax−solvent mixture, at an inlet temperature, T_{hi} > WAT, through a short tube of length L, with the inside and outside radii, R_i and R_o, respectively. It is cooled by a "cold" water stream at an inlet temperature, T_{ci} < WAT, flowing counter-currently through the annular region of the double-pipe heat exchanger, with an outside radius of R_j. The outlet hot and cold stream temperatures are T_{ho} (<T_{hi}) and T_{co} (>T_{ci}), respectively. The mass flow rates, specific heat capacities, densities, and heat-transfer coefficients of the wax−solvent mixture and coolant (water) are m_h, C_h, ρ_h, and h_i and m_c, C_c, ρ_c, and h_o, respectively. The deposit formation on the inner tube wall would commence once the inside tube-wall temperature, T_{wi}, is below the WAT, while the liquid−deposit interface temperature, T_d, remains at the WAT.

Using s (=$R_i - \delta$) to denote the radial location of the liquid−deposit interface at time t, the energy balance equation for the wax−solvent solution, at T_h > WAT, flowing through the tube is

$$m_h C_h (T_{hi} - T_{ho}) = (2\pi sL) h_i (T_h - T_d) + (\pi s^2 L) \rho_h C_h \frac{dT_h}{dt} \quad (1)$$

Similarly, the energy balance equation for the coolant (water) in the annular region is

$$m_c C_c (T_{co} - T_{ci}) = (2\pi R_o L) h_o (T_{wo} - T_c) + (\pi L)(R_j^2 - R_o^2) \rho_c C_c \frac{dT_c}{dt} \quad (2)$$

In eqs 1 and 2, all properties of the wax−solvent mixture and the coolant are taken at their average temperatures, T_h and T_c, respectively.

In the moving boundary problem approach, the deposit-layer growth is governed by heat-transfer at the liquid−deposit interface. For the deposit layer, at t > 0, because $T = T_d$ at $r = s$ and $T = T_{wi}$ at $r = R_i$, therefore, $(\partial T_\delta/\partial z) = \partial^2 T_\delta/\partial z^2 = 0$. That is, within the deposit layer, the rate of heat flow in the axial direction was neglected. The energy balance equation for the deposit layer is

(26) Coutinho, J. A. P. Predictive UNIQUAC: A New Model for the Description of Multiphase Solid−Liquid Equilibria in Complex Hydrocarbon Mixtures. *Ind. Eng. Chem. Res*. **1998**, *36*, 4870.

$$\frac{1}{r}\frac{\partial}{\partial r}\left(r\frac{\partial T_\delta}{\partial r}\right) = \frac{1}{\alpha'_\delta}\frac{\partial T_\delta}{\partial t} \quad s < r < R_i, z > 0 \tag{3}$$

where T_δ is the deposit-layer temperature. α'_δ in eq 3 represents a modified thermal diffusivity of the deposit layer, as follows:[22,23]

$$\frac{1}{\alpha'_\delta} = \frac{1}{\alpha_\delta} - \frac{\rho\lambda}{k_d}\frac{\partial f}{\partial T_\delta} \tag{4}$$

where α_δ is the deposit thermal diffusivity, f is the solid-phase fraction in the deposit, λ is the latent heat of freezing, and k_d is the average deposit thermal conductivity.

The energy balance at the liquid−deposit interface is[22,23]

$$k_d\frac{\partial T_\delta}{\partial r} - h_i(T_h - T_d) = \rho\lambda f_s\frac{ds}{dt} \quad r = s \tag{5}$$

where f_s is the equilibrium solid-phase fraction at the liquid−deposit interface (i.e., at $r = s$) corresponding to the liquid−deposit interface temperature, T_d.

The boundary and initial conditions for eqs 1−3 and 5 are

$$T_\delta = T_d \quad r = s, t > 0 \tag{6a}$$

$$T_\delta = T_{wi} \quad r = R_i, t > 0 \tag{6b}$$

$$T_h = T_{hi} \quad t = 0 \tag{6c}$$

$$T_c = T_{hi} \quad t = 0 \tag{6d}$$

$$s = R_i \quad t = 0 \tag{6e}$$

Neglecting the heat capacity of the tube wall, the conduction equation for the pipe wall is

$$\frac{1}{r}\frac{\partial}{\partial r}\left(r\frac{\partial T_m}{\partial r}\right) = 0 \tag{7}$$

where T_m denotes the tube-wall temperature. The boundary conditions for eq 7 are

$$\text{At } T_{wi} < \text{WAT: } -k_d\frac{\partial T_d}{\partial r} = -k_m\frac{\partial T_m}{\partial r} \quad r = R_i \tag{8a}$$

$$\text{At } T_{wi} > \text{WAT: } h_i(T_h - T_{wi}) = -k_m\frac{\partial T_m}{\partial r} \quad r = R_i$$

$$-k_m\frac{\partial T_m}{\partial r} = h_o(T_{wo} - T_c) \quad r = R_o \tag{8b}$$

Description of the Wax−Solvent Mixtures. As mentioned previously, the deposition experiments of Bidmus and Mehrotra[15] were performed with prepared solutions of a multicomponent wax dissolved in high-purity *n*-$C_{12}H_{26}$. The wax sample, with a melting point of about 58−62 °C, consisted of *n*-alkanes ranging from $C_{20}H_{42}$ to $C_{40}H_{82}$. The average molar mass of the wax sample was calculated as 390.8 kg/kmol, which corresponds to a mean carbon number of 28.[15,24] The deposition experiments by Parthasarathi and Mehrotra[16] were performed with prepared solutions of the same wax dissolved in Norpar13. Norpar13 is a mixture of *n*-alkanes, ranging from C_9H_{20} to $C_{16}H_{34}$, with $C_{13}H_{28}$ and $C_{14}H_{30}$ being its two predominant constituents. The average molar mass of Norpar13 was calculated as 185.7 kg/kmol, which corresponds to a mean carbon number of about 13.[16,25]

Thermodynamic Calculations. All liquid−solid-phase equilibrium calculations were performed using the predictive UNIQUAC model,[26] which includes a modification to account for the solid-phase nonideality in the original UNIQUAC model. The same model was also used in our previous study for comparing the experimental wax disappearance temperature (WDT) with the predicted liquidus temperature of wax−solvent mixtures.[27] The results in this study were obtained by use of the melting-point temperature correlation by Broadhurst,[28] instead of that given by Coutinho.[26]

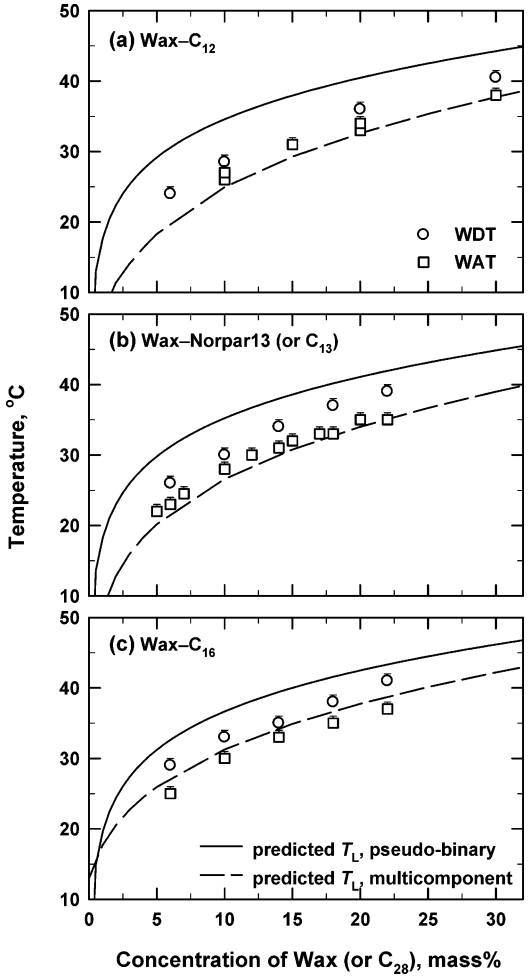

Figure 1. Comparison of WDT and WAT data[15,16,27] with the predicted liquidus temperature, T_L, for three wax−solvent mixtures using eutectic pseudo-binary and multicomponent liquid−solid-phase equilibrium models: (a) wax−$C_{12}H_{26}$ mixtures,[15] (b) wax−$C_{13}H_{28}$ mixtures,[16,27] and (c) wax−$C_{16}H_{34}$ mixtures.[27]

Figure 1 shows the effect of the wax concentration on the experimental WAT and WDT for three wax−solvent mixtures, namely, wax−C_{12},[15] wax−Norpar13,[16] and wax−C_{16}.[27] The data are compared with the predictions from Coutinho's model.[26] Also shown are the predictions for the liquidus temperature, T_L, obtained by approximating each mixture as a binary eutectic mixture of two pseudo-components, i.e., $C_{28}H_{58}$−$C_{12}H_{26}$ in Figure 1a, $C_{28}H_{58}$−$C_{13}H_{28}$ in Figure 1b, and $C_{28}H_{58}$−$C_{16}H_{34}$ in Figure 1c. In all cases, the predicted T_L from the eutectic pseudo-binary approximation is higher than the WDT. The predicted T_L for the multicomponent mixtures from the Coutinho model[26] is lower than the WDT, particularly for the wax−$C_{12}H_{26}$ and wax−Norpar13 mixtures in parts a and b of Figure 1.

Estimation of Liquid and Deposit Properties. All liquid-phase and deposit-layer properties were estimated using the methods described previously.[22] All liquid-phase properties were estimated at the average temperature, i.e., $(T_h + T_d)/2$. The thermal conductivity of the deposit layer was obtained by matching the experimental deposit mass. The density changes caused by the partial solidifica-

(27) Bhat, N. V.; Mehrotra, A. K. Measurement and Prediction of the Phase Behavior of Wax−Solvent Mixtures: Significance of the Wax Disappearance Temperature. *Ind. Eng. Chem. Res.* **2004**, *43*, 3451.

(28) Broadhurst, M. G. An Analysis of the Solid Phase Behavior of the Normal Paraffins. *J. Res. Natl. Bur. Stand., Sect. A* **1962**, *66*, 241.

tion at the liquid−deposit interface and in the deposit layer were neglected.

Numerical Solution Methodology. For the deposition calculations, eqs 1−3, 5, and 7 together with the boundary and initial conditions were solved numerically to obtain the time-dependent variations of average liquid temperatures, T_h and T_c, the tube-wall temperatures, T_{wi} and T_{wo}, the temperature profile across the deposit layer, T_δ, and the location of the liquid−deposit interface, s. Using the numerical solution methodology described elsewhere,[22] all differential equations were discretized using the explicit method, in which the dependent variables were estimated from their known values at the previous time interval. The domain $0 < r < R_i$ was divided into n equally spaced concentric rings of Δr thickness, i.e., $\Delta r = R_i/n$. The values of Δr and Δt were selected to satisfy the following stability criterion:

$$(\alpha \Delta t)/(\Delta r)^2 \leq 1/2 \tag{9}$$

To economize on the computational time, n ($\equiv R_i/\Delta r$) = 150 was chosen, which was estimated to yield an error of less than 0.5% in the deposit-layer thickness. The magnitudes of Δr and Δt were selected accordingly for obtaining the results presented in this study.

Cubical-Cage Representation for Modeling the Effect of Shear Stress. The effect of shear stress caused by the flowing wax−solvent mixture on the deposition process was ignored in our previous modeling studies.[22,23] More recent studies have shown that the paraffin crystal aggregation during gel formation can be affected by even low shear stresses.[4] It is pointed out that, without including the effect of shear stress, the overall deposit composition would be the same as that of the wax−solvent mixture, even though the ratio of solid and liquid phases present in the deposit might be altered because of changes in the temperature. This is contrary to the experimental evidence,[15,16] which indicated that the deposit has a higher concentration of C_{20}^+ *n*-alkanes than the wax−solvent mixture. Moreover, the experimental results also suggested that the change in deposit composition is dependent upon the flow rate (or shear stress) such that a higher deposit wax content is achieved at higher Reynolds numbers.[15,16] That is, an enrichment of C_{20}^+ *n*-alkanes and/or a depletion of C_{20}^- *n*-alkanes would occur during the deposition process.

For including the effect of shear stress or Reynolds number on the deposition process, we propose a simplified representation of the deposit. It is emphasized that the proposed representation does not intend to match the configuration in which the solid and liquid phases might actually coexist in the gel-like deposit. Also, it does not attempt to describe the crystalline or structured nature of the solid phase within the deposit. Moreover, it is pointed out that the proposed representation does not relate to the process of nucleation and growth involved in wax deposition. Rather, its sole purpose is to provide a quantitative measure for the effect of Reynolds number or shear stress on the relative amounts of solid and liquid phases in the deposit. Furthermore, even though the effect of shear stress is modeled via the formation of a cubical cage under static conditions, involving heat-transfer and phase equilibrium considerations, followed by squeezing out a part of the liquid-phase because of its tilting caused by shear stress, these two processes would occur simultaneously during deposition.

Recognizing that the gel-like deposit consists of liquid and solid phases, let us visualize the deposit layer under static conditions (i.e., without the presence of any shear stress) to comprise a lattice-like structure with a unit cell that resembles a cage, in which the solid phase is confined to the edges, while the liquid-phase occupies the remaining space. To keep the mathematical analysis simple, each unit cell or cage is assumed to be a cube. As shown in Figure 2a, the unit cell under static conditions is a cubical cage, $a \times a \times a$, in which each edge is a rectangular member, $\xi \times \xi$ in the cross-section. The edge thickness to the cube side ratio of the unit cell is $Z = \xi/a$. The total volume of the cubical cage is $V = a^3$. The solid-phase volume fraction in the cubical cage is $V_S = (12Z^2 - 16Z^3)$. The liquid-phase volume fraction, by difference, is $V_L = (1 - 12Z^2 + 16Z^3)$. Note that the two extreme cases for the solid and liquid volume fractions are $V_S = 0$, $V_L = 1$ for $Z = 0$ (i.e., no solid phase present) and $V_S = 1$, $V_L = 0$ for $Z = 0.5$ (i.e., no liquid phase present). Figure 3 shows the relationships of V_S and V_L with Z ($=\xi/a$).

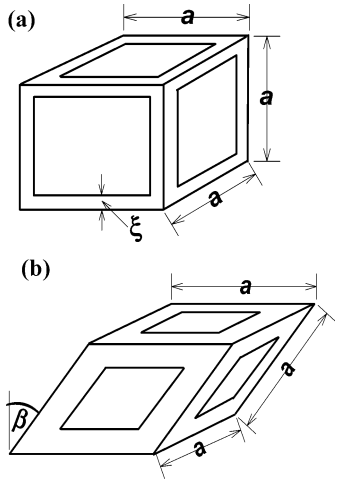

Figure 2. Schematic of the cubical-cage representation: (a) cubical cage (untilted, under static conditions) and (b) tilted cage (at a deformation angle of β).

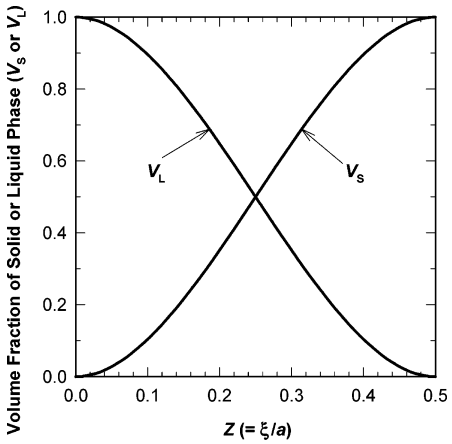

Figure 3. Changes in the solid- and liquid-phase fractions in the cubical cage under static conditions (i.e., $\beta = 0$, untilted) with Z ($=\xi/a$).

As shown in Figure 2b, the application of a one-dimensional shear stress, because of the flow in the horizontal direction, is assumed to cause the cubical cage to tilt by an angle β (measured from the vertical plane) such that it is transformed into a monoclinic-type geometry. As shown in Figure 2b, the top, bottom, left, and right faces of the tilted cage are squares and the front and back faces are rhombi. The length of each edge of the tilted cage remains the same, but its total volume decreases, while the solid-phase volume during the tilting of the cubical cage is conserved. The volume of the tilted cage, with the deformation angle of β, is $V_\beta = V \sin(\pi/2 - \beta) = a^3 \cos \beta$. Because the solid-phase volume is conserved during deformation, the solid-phase volume fraction in the tilted cage is $V_{S\beta} = (V_S \times V)/V_\beta = (12Z^2 - 16Z^3)/(\cos \beta)$. The liquid-phase volume fraction in the tilted cage is $V_{L\beta} = [1 - (12Z^2 - 16Z^3)/(\cos \beta)]$. The volume change for the liquid phase, as a result of the tilting, is $a^3(1 - \cos \beta)$, and the relative volume change for the liquid phase compared to the original liquid volume is $-\Delta V_L/V_L = (1 - \cos \beta)/(1 - 12Z^2 + 16Z^3) = (1 - \cos \beta)/[(1 + 4Z)(1 - 2Z)^2]$. Note that $V_{L\beta} = 0$ at $\beta = \cos^{-1}(12Z^2 - 16Z^3)$, which corresponds to the complete release of all of the liquid phase from the tilted cage. That is, $\beta \leq \cos^{-1}(12Z^2 - 16Z^3)$.

It is noted that all of the above relationships are expressed in terms of parameter Z; i.e., they are independent of the size of the cubical cage. Moreover, Z in all of the above relationships

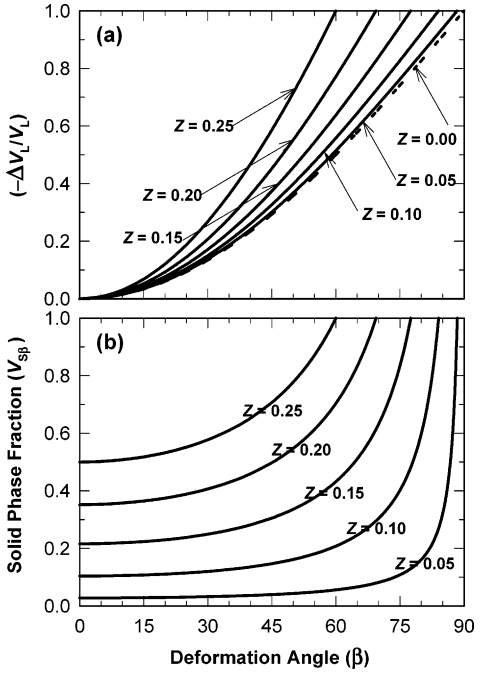

Figure 4. Effect of the deformation angle, β, on the relative liquid-phase volume change, $-\Delta V_L/V_L$, and the solid-phase fraction, $V_{S\beta}$, at selected Z.

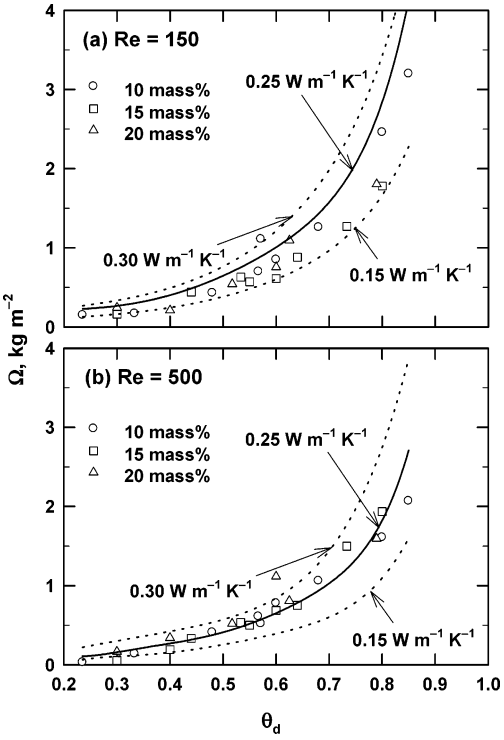

Figure 5. Effect of k_d on the relationship between Ω and θ_d, with data from Bidmus and Mehrotra.[15]

corresponds to the cubical cage, i.e., the unit cell under static conditions without any shear stress. Thus, Z is estimated directly from the liquid−solid-phase equilibrium calculations at the temperature of the cubical cage.

Figure 4 shows the effect of the tilted-cage deformation angle, β, on the relative change in the liquid-phase volume and the solid-phase fraction at selected values of Z ranging from 0 to 0.25. In Figure 4a, the relative change in the liquid-phase volume, $-\Delta V_L/V_L$, increases more gradually with an increase in β for all values of Z. Also, the maximum possible deformation angle decreases with an increase in Z. In Figure 4b, however, the solid-phase fraction does not change much until the deformation angle reaches within about 30° of its highest possible limit. That is, the deformation angle would have to be relatively large to achieve a significant increase in the solid-phase fraction in the deposit.

Parameters Z and β. The relationships for the cubical-cage representation involve only two parameters, namely, the edge thickness to the cube side ratio, Z ($=\xi/a$), and the deformation angle, β. The numerical value of parameter Z for the untilted cubical cage depends upon the fraction of solid phase formed from a wax−solvent mixture, which as mentioned previously would be dictated by the liquid−solid-phase equilibrium at the deposition temperature. Because Z depends upon the composition of the wax−solvent mixture and the liquid−deposit interface temperature, its value cannot be manipulated. The deformation angle, β, is expected to depend upon Re or shear stress and possibly other variables; hence, it could be estimated from experimental data.

The use of the experimental deposit composition to estimate β is an inverse problem, which required a large number of trial-and-error calculations with different values of β. To simplify the task of estimating β, it was assumed that the deformation of the cubical cage occurs only when a layer of deposit is formed initially. That is, the effect of shear stress was assumed to be only on the newly formed layer and not on the previously formed layers buried beneath it. In other words, the composition of each layer was not altered for the subsequent time intervals. However, the liquid−solid-phase equilibrium calculations were repeated as the deposit temperature profile changed with time and increased deposition, which caused a small change in the liquid/solid ratio in each layer. The optimum β was selected by matching the predicted average wax content of the deposit layer with that found experimentally.

Results and Discussion

Calculations were performed at the conditions of the deposition experiments,[15,16,24,25] summarized in Tables 1 and 2. Even though only the average Reynolds numbers are listed in Table 1 and 2, the actual flow rates[24,25] of the wax−solvent mixtures were used in these calculations. For all cases, the time taken to reach the steady state was found to be a few minutes, which is in agreement with the experimental observation that the thermal steady state was accomplished within 20−30 min.[15,24] The predicted results for the mass of the deposit layer at the steady state were compared with the experimental data, expressed as the deposit mass per unit area, Ω.

Importance of Deposit Thermal Conductivity, k_d. Preliminary calculations indicated that the predicted Ω was most sensitive to the deposit thermal conductivity, k_d. Parts a and b of Figure 5 present the variation of Ω with the fractional deposit thermal resistance, θ_d, at average Reynolds numbers of 150 and 500, respectively. The symbols in Figure 5 represent the experimental results obtained at different T_h and T_c with the 10, 15, and 20 mass % wax−$C_{12}H_{26}$ mixtures.[15,24] The curves in Figure 5 represent the predictions for three average k_d values, ranging from 0.15 to 0.30 W m^{-1} K^{-1}. It is clear from the results in Figure 5 that a variation in k_d has a significant effect on the predicted deposit-layer mass. This is because the mathematical expression for the deposit-layer thermal resistance contains both k_d and the average deposit-layer thickness, δ; i.e., $R_d = [\ln\{R_i/(R_i - \delta)\}/(2\pi L k_d)]$. For the same R_d (and the same θ_d), a lower deposit thermal conductivity underpredicted the deposit mass.

In Figure 5, both the data and predictions do not indicate any dependence of Ω on the composition of wax−solvent mixtures; that is, Ω is dependent upon only the fractional thermal resistance of the deposit, θ_d.[15,16] Even though $k_d = 0.25$ W m^{-1} K^{-1} provided a good overall match for both sets of data in Figure 5, the use of the average k_d for all experiments in Tables 1 and 2 yielded relatively large errors in the predicted Ω. It

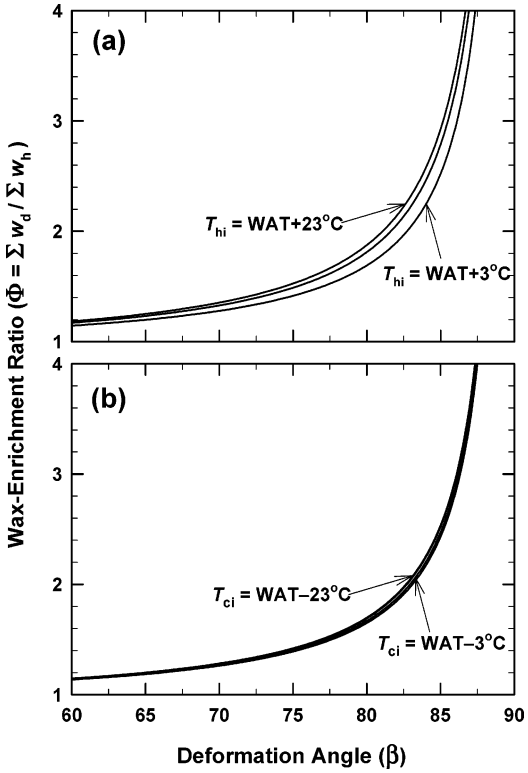

Figure 6. Predicted effect of the deformation angle, β, on the wax-enrichment ratio, Φ, for a 10 mass % wax−$C_{12}H_{26}$ mixture at Re = 500, T_{hi} = WAT + 3 °C, and T_{ci} = WAT − 17 °C: (a) sensitivity of predictions to T_{hi} and (b) sensitivity of predictions to T_{ci}.

was, therefore, decided to estimate k_d for each experiment by matching the experimentally measured Ω.

Effect of the Deformation Angle, β, on Deposit-Layer Composition. Calculations were performed to study the effect of the deformation angle, β, on the deposit-layer composition. All of these calculations for the 10 mass % wax−$C_{12}H_{26}$ mixture were for one set of experimental conditions corresponding to the first entry in Table 1, i.e., Re = 500, T_{hi} = WAT + 3 °C, and T_{ci} = WAT − 17 °C. For an effective comparison of the wax content in the deposit layer with that in the wax−solvent mixture, a wax-enrichment ratio, Φ, is defined as follows:[16]

$$\Phi = \sum_{j=20}^{40} (w_d)_j / \sum_{j=20}^{40} (w_h)_j \qquad (10)$$

In eq 10, $(w_d)_j$ denotes the mass fraction of the jth n-alkane in the deposit and $(w_h)_j$ denotes the mass fraction of the jth n-alkane in the wax−solvent mixture. Note that $\sum(w_h)_j$ for the 10 mass % wax−solvent mixture is 0.1. Accordingly, for the 10 mass % wax−solvent mixture, Φ can vary between 1.0 (for no wax enrichment in the deposit) to 10.0 (for the deposit to be 100% wax or totally devoid of any solvent). It is interesting to point out that Φ = 1.0 corresponds to $\beta = 0°$, which would be the case for the deposit (or gel) formed under static conditions. On the other hand, Φ = 10.0 would occur at the maximum possible deformation of the cubical cage for which $\beta = \cos^{-1}(12Z^2 - 16Z^3)$ is the upper limit, as derived before. Obviously, the upper limit of β would approach 90° (or $\pi/2$) as $Z \rightarrow 0$, which represents the extreme case where the cubical cage consists of only the liquid phase. As shown in the first entry in Table 1, β was predicted to be 79.2° for Φ = 1.62.

The results of calculations, for $\beta > 60°$, are shown in Figure 6. All of the curves are similar in shape to that for $Z = 0.05$ in Figure 4b. In Figure 6a, in addition to the predictions for T_{hi} = WAT + 3 °C, results are also shown for T_{hi} = WAT + 13 °C and WAT + 23 °C. The predictions indicated that, for the same β, an increase in T_{hi} leads to a higher wax-enrichment ratio or a higher wax content in the deposit. For example, at $\beta = 80°$, an increase in T_{hi} from 30 to 50 °C was predicted to increase Φ from 1.69 to 1.85.

In Figure 6b, predictions are shown for three T_{ci}, i.e. WAT − 3 °C, WAT − 17 °C, and WAT − 23 °C. Even though the difference between these curves is not as much as in Figure 6a, the predictions indicated that, for the same β, a decrease in the coolant temperature leads to a slightly higher wax-enrichment ratio or a higher wax content in the deposit. For example, at $\beta = 80°$, a decrease in T_{ci} from 24 to 4 °C was predicted to increase Φ slightly from 1.65 to 1.69.

Overall, these predictions indicated that the deposit formed at a higher T_h and a lower T_c would have a higher wax content, which is expected to be "harder" with a more solid-like gel. Conversely, the deposit formed at both T_h and T_c held close to the WAT would have a lower wax content, which is expected to be "softer" with a more liquid-like gel. These predictions are supported by similar observations made in the experimental studies.[15,16,24,25]

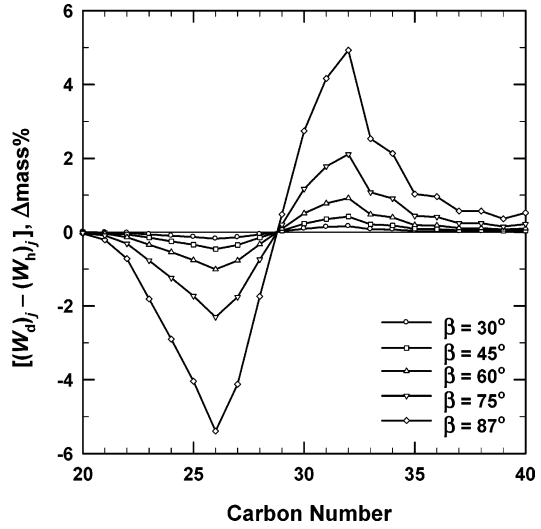

Figure 7. Effect of the deformation angle, β, on predicted differences between the normalized concentrations of n-alkanes in the deposit layer and wax−solvent mixture $[(W_d)_j - (W_h)_j]$; predictions for a 10 mass % wax−$C_{12}H_{26}$ mixture at Re = 500, T_{hi} = WAT + 3 °C, and T_{ci} = WAT − 17 °C.

The predicted deposit compositions were also evaluated for changes in the concentration of each n-alkane in the wax, i.e., from $C_{20}H_{42}$ to $C_{40}H_{82}$. All calculations were made for the experimental conditions corresponding to the first entry in Table 1, i.e., a 10 mass % wax−$C_{12}H_{26}$ mixture at Re = 500, with T_{hi} = WAT + 3 °C, T_{ci} = WAT − 17 °C, and k_d = 0.24 W m^{-1} K^{-1}. Because all of these calculations were made at identical conditions with the same k_d, the predicted deposit mass was the same for all cases. To express the change in n-alkane content, the concentrations of each carbon number, from 20 to 40, in the deposit and the wax−solvent mixture were first normalized, which are denoted by W_d and W_h, respectively. The predicted differences between the two normalized concentrations $[(W_d)_j - (W_h)_j]$ are plotted in Figure 7 against the carbon number for five arbitrarily selected values of β. It is pointed out that the symbols have been used in Figure 7 only for identifying the different curves; i.e., they do not represent any experimental data.

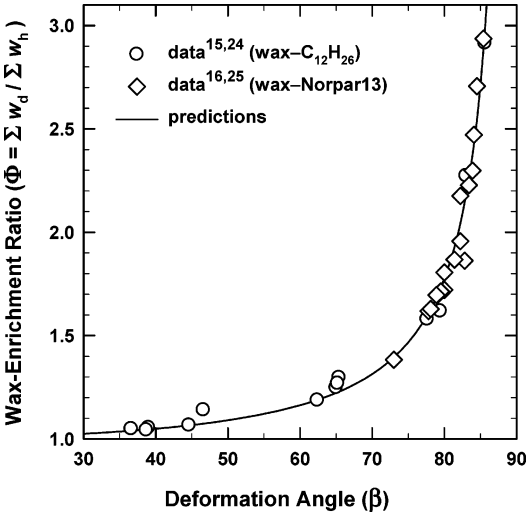

Figure 8. Comparison of the experimental[15,16,24,25] and predicted dependence of the wax-enrichment ratio, Φ, on estimated β for wax−$C_{12}H_{26}$ and wax−Norpar13 mixtures; predictions for a 10 mass % wax−$C_{12}H_{26}$ mixture at Re = 500, T_{hi} = WAT + 3 °C, and T_{ci} = WAT − 17 °C.

Three observations can be made from the predicted trends shown in Figure 7. First, the deposit corresponding to each β is enriched in the heavier *n*-alkanes and depleted in the lighter *n*-alkanes. That is, the cubical-cage deformation causes a change in the liquid-phase content in the deposit such that the lighter *n*-alkanes are released preferentially, which causes a corresponding increase in the concentration of heavier *n*-alkanes. Second, an increase in β is predicted to cause an increased enrichment of the heavier *n*-alkanes and an increased depletion of the lighter *n*-alkanes. Finally, all of the curves for different deformation angles intersect the abscissa (i.e., 0.0 Δmass %) at exactly the same carbon number of about 28−29. Note that this carbon number is also close to the average carbon number of the original wax, which is about 28.[15,16]

Estimation of the Deformation Angle, *β*, for All Experimental Data. The above calculations were repeated for all of the deposition experiments in Tables 1 and 2 with both wax−$C_{12}H_{26}$ and wax−Norpar13 mixtures, respectively. For each deposition run, the experimental conditions along with θ_d, Ω, k_d, Φ, and the estimated β are listed in Tables 1 and 2. It was noticed that the GC analysis of deposit samples from all of the experiments with the 15 and 20 mass % wax−$C_{12}H_{26}$ mixtures in Table 1 indicated much lower wax contents, as shown by the low values of Φ, which gave relatively lower values of the estimated β. For these experiments, however, the results for θ_d, Ω, and k_d did not show any such inconsistency. This observation suggests that an error might have occurred in collecting the deposit samples or in their GC analysis.

Plotted in Figure 8 are all of the results in Tables 1 and 2 for the wax-enrichment ratio, Φ, against the estimated deformation angle, β. The smooth curve in Figure 8 represents the predictions for the single experiment with a 10 mass % wax−$C_{12}H_{26}$ mixture (at Re = 500, with T_{hi} = WAT + 3 °C, T_{ci} = WAT − 17 °C, and k_d = 0.24 W m^{-1} K^{-1}). The good agreement between the data and predictions is viewed as a confirmation of the cubical-cage-deformation approach.

Figure 9 shows the differences in the normalized concentrations of each *n*-alkane in the deposit sample and the corresponding wax−Norpar13 mixture. The data points shown in Figure 9 are taken from Figure 13 of Parthasarathi and Mehrotra,[16] and these represent the averages of all 4 h deposition experiments performed with the four wax−Norpar13 mixtures.

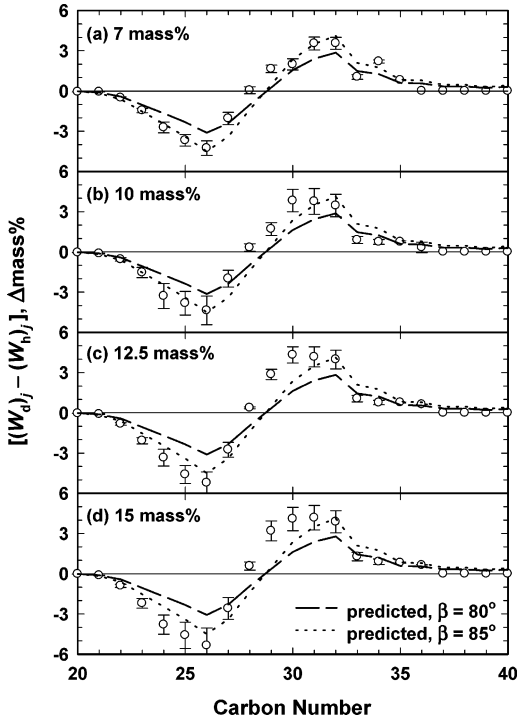

Figure 9. Comparison of the experimental[16] and predicted differences between the normalized concentrations of *n*-alkanes in the deposit layer and wax−Norpar13 mixture $[(W_d)_j - (W_h)_j]$; predictions for a 10 mass % wax−Norpar13 mixture at Re = 1000, T_{hi} = WAT + 5 °C, and T_{ci} = WAT − 10 °C at β = 80° and 85°.

In Table 2, the estimated β for these experiments varies from about 80° to 85°. The two curves in all plots of Figure 9 represent the predictions at β = 80° and 85° for Re = 1000, T_{hi} = WAT + 5 °C, and T_{ci} = WAT − 10 °C. The predictions are seen to match the data quite well. Also, in Figure 9, the trends in the data and predictions for all four wax−solvent mixtures are qualitatively and quantitatively similar. This suggests that the differences in carbon-number distributions do not depend upon the wax concentration, provided that the two temperature differences (or thermal driving forces), (T_h − WAT) and (WAT − T_c), are similar for the different wax−solvent mixtures. Figure 9 also indicates that all of the curves for the normalized concentrations of *n*-alkanes intersect the abscissa at a carbon number of about 28−29, which is identical to that observed in the predicted curves in Figure 7 for the wax−$C_{12}H_{26}$ mixture.

Correlation of the Deformation Angle, *β*. After the cubical-cage-deformation approach was validated to represent the effect of shear stress on deposit composition, an attempt was made to correlate β with other variables that can be measured or estimated reliably, such as θ_d, Ω, and Re. Because of the concern raised previously, all of the estimated β values for the 15 and 20 mass % wax−$C_{12}H_{26}$ mixtures in Table 1 were excluded from further analysis.

The results for the wax−Norpar13 mixtures, in Table 2, are plotted in Figure 10. Despite the scatter, the data in Figure 10a suggest an inverse relationship between θ_d and β. With the tube-wall and outside (water) convective resistances being relatively small,[16] it can shown that $\theta_d \approx (T_d - T_c)/(T_h - T_c)$. Hence, θ_d could be estimated easily from the temperature measurements. Thus, a correlation between β and θ_d would be useful for predicting deposit properties. The data in Figure 10b indicate a similar inverse relationship between Ω and β. That is, the higher the Ω, the lower the β. A higher Ω implies a thicker deposit layer, while a lower β corresponds to a deposit that has a lower wax content or a higher liquid-phase fraction. Even though the

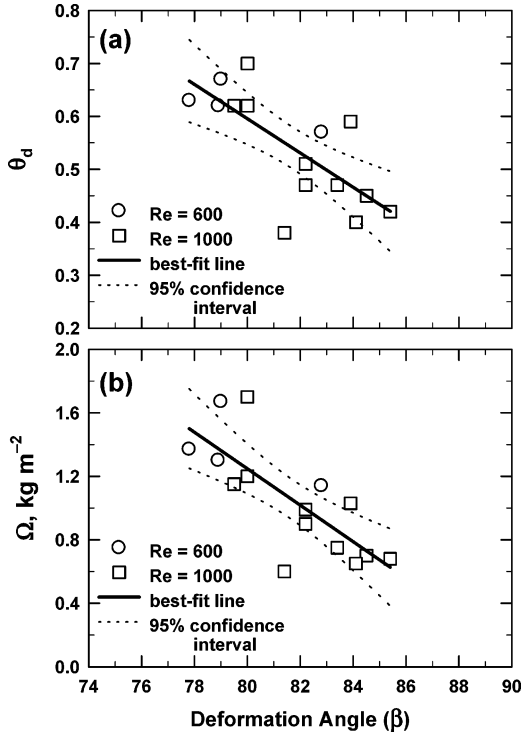

Figure 10. Correlation of the estimated β (a) with θ_d and (b) with Ω, with data from Parthasarathi and Mehrotra.[16]

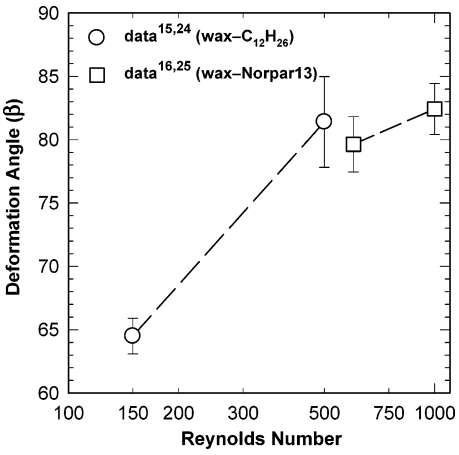

Figure 11. Correlation of the estimated β with Re for the short tube lengths, with data from Bidmus and Mehrotra,[15] Parthasarathi and Mehrotra,[16] Bidmus,[24] and Parthasarathi.[25]

trends in parts a and b of Figure 10 are correct and consistent, a correlation is not proposed because of the apparent scatter in the available data.

In Figure 11, the estimated deformation angles from the data of both deposition studies are plotted against the logarithm of Reynolds number for the short tube lengths used in the experiments. The trend in Figure 11 suggests an increase in β with an increase in Re. With a direct proportionality between Re and shear stress (at the wall) for laminar flow, a higher Re implies a higher shear stress. The observed increase in β with an increase in shear stress provides further support for the cubical-cage-deformation approach proposed in this study.

Clearly, the trends shown in Figures 10 and 11 need to be established with a much greater statistical confidence level. This would require additional deposition data on similar prepared mixtures and "waxy" crude oils under laminar and turbulent flow regimes. Furthermore, deposition experiments performed over different deposition periods would be useful for establishing changes in β with time. The additional data would be useful for extending and further validating the cubical-cage-deformation approach of this study, over a wider range of Reynolds numbers and operating conditions.

Conclusions

A mathematical model based on the moving boundary problem approach for heat transfer with a phase change was presented for the solids deposition from waxy mixtures under laminar flow. The differential equations were solved numerically to predict the deposit-layer thickness for two wax−solvent mixtures over a range of experimental conditions. The predictions were compared with the data from two recent laboratory deposition studies under laminar flow.

A novel representation, involving the one-dimensional deformation of a cubical cage, was proposed for incorporating the effect of shear stress on the deposition process. The extent of cubical-cage deformation influenced the liquid/solid ratio, while the deposition occurs at the liquid−solid interface. Thus, the cubical-cage-deformation approach afforded a means for estimating the optimum deformation angle, β, that corresponds to the deposit-layer composition. The proposed cubical-cage-deformation approach, coupled with the heat-transfer and thermodynamic considerations, provided a good match of the experimental deposition results.

The predictions indicated that the deposition at higher T_h would yield a lower mass of a "harder" and more solid-like deposit with a higher wax-enrichment ratio. Conversely, the deposition at T_h held close to the WAT was predicted to yield a higher mass of a "softer" and more liquid-like deposit with a lower wax-enrichment ratio. The wax-enrichment ratio, however, was not as sensitive to a change in T_c. An increase in the deformation angle was shown to cause a shift in the carbon-number distribution for the *n*-alkanes contained in the deposit, and the predicted trends were in agreement with the published data. The predictions at the estimated deformation angle indicated that *n*-alkanes heavier than C_{29} were enriched in the deposit, whereas those lighter than C_{28} were depleted in the deposit. This carbon number of $C_{28}-C_{29}$ was noted to be close to the average carbon number of about C_{28} for the original wax.

The tilted-cage deformation angle, β, was shown to be related to the fractional deposit thermal resistance (or the fractional temperature drop), θ_d, the deposit mass per area, Ω, and the Reynolds number of the deposit-forming wax−solvent mixture. The deposit composition was predicted to be influenced by shear stress and thermodynamic considerations. An increase in β caused wax enrichment of the deposit layer without affecting the deposit-layer thickness, which is governed by heat-transfer and phase equilibrium considerations. The agreement between the predicted trends and the experimental results provided further support for the deposition process to be primarily thermally driven.

Acknowledgment. Financial support was provided by the Natural Sciences and Engineering Research Council of Canada (NSERC) and the Department of Chemical and Petroleum Engineering, University of Calgary, Calgary, Alberta, Canada. We acknowledge the support from member universities of Westgrid Network, Canada, for allowing the use of their computation facilities.

Nomenclature

C_c = specific heat capacity of the coolant (water), J kg^{-1} K^{-1}
C_h = specific heat capacity of the wax−solvent mixture, J kg^{-1} K^{-1}

f = mass fraction of the solid phase in the deposit
f_s = mass fraction of the solid phase at the liquid−deposit interface
h_i = inside heat-transfer coefficient for the wax−solvent mixture, W m^{-2} K^{-1}
h_o = outside heat-transfer coefficient for the coolant (water), W m^{-2} K^{-1}
j = jth n-alkane in the wax
k_m = thermal conductivity of tube metal, W m^{-1} K^{-1}
k_d = average thermal conductivity of the deposit, W m^{-1} K^{-1}
L = tube length, m
m_c = mass flow rate of the coolant (water), kg s^{-1}
m_h = mass flow rate of the wax−solvent mixture, kg s^{-1}
n = number of radial divisions ($=R_i/\Delta r$)
r = radial distance, m
R_c = thermal resistance offered by the coolant, K W^{-1}
R_d = thermal resistance offered by the deposit, K W^{-1}
R_h = thermal resistance offered by the wax−solvent mixture, K W^{-1}
R_i = tube inside radius, m
R_j = outside radius of the annular region, m
R_m = thermal resistance offered by the tube wall, K W^{-1}
R_o = tube outside radius, m
Re = Reynolds number
s = radial location of liquid−deposit interface, m
t = time, s
T_c = average temperature of the coolant (water), °C
T_{ci} = inlet coolant temperature, °C
T_{co} = outlet coolant temperature, °C
T_d = liquid−deposit interface temperature, °C
T_δ = deposit-layer temperature, °C
T_h = average temperature of the wax−solvent mixture, °C
T_{hi} = inlet wax−solvent mixture temperature, °C
T_{ho} = outlet wax−solvent mixture temperature, °C
T_L = liquidus temperature, °C
T_m = tube-wall temperature, °C
T_{wi} = average inside tube-wall temperature, °C
T_{wo} = average outside tube-wall temperature, °C
V = volume of the cubical cage, m^3
V_L = volume fraction of the liquid phase in the cubical cage
V_S = volume fraction of the solid phase in the cubical cage
V_β = volume of the tilted cage (deformation angle = β), m^3
$V_{L\beta}$ = volume fraction of the liquid phase in the tilted cage
$V_{S\beta}$ = volume fraction of the solid phase in the tilted cage
w_d = mass fraction of C_{20}^+ n-alkane in the deposit
W_d = normalized mass fraction of C_{20}^+ n-alkane in the deposit
w_h = mass fraction of C_{20}^+ n-alkane in the wax−solvent mixture
W_h = normalized mass fraction of C_{20}^+ n-alkane in the wax−solvent mixture
z = axial distance, m

Greek Letters

α = thermal diffusivity of the deposit, m^2 s^{-1}
α'_δ = apparent thermal diffusivity of the deposit, m^2 s^{-1}
β = deformation angle of the tilted cage
ρ = density, kg m^{-3}
δ = deposit-layer thickness, m
λ = latent heat of fusion, J kg^{-1}
θ_d = fractional thermal resistance (or fractional temperature drop) of the deposit at the steady state
Ω = mass of the deposit per unit inside tube surface area, kg m^{-2}
Φ = wax-enrichment ratio $\equiv \sum(w_d)_j/\sum(w_h)_j$

Acronyms

PPT = pour point temperature, °C
WAT = wax appearance temperature, °C
WDT = wax disappearance temperature, °C

EF060445U